

Giant magnetic domains in amorphous SmCo thin filmsFridrik Magnus,^{1,*} Reda Moubah,¹ Unnar B. Arnalds,¹ Vassilios Kapaklis,¹ Anna Brunner,² Rudolf Schäfer,² Gabriella Andersson,¹ and Björgvin Hjörvarsson¹¹*Department of Physics and Astronomy, Uppsala University, Box 516, 751 20 Uppsala, Sweden*²*Institute for Materials Science, TU Dresden, 01069 Dresden, Germany*

(Received 25 April 2014; revised manuscript received 11 June 2014; published 30 June 2014)

The potential for tuning of magnetic properties and the exceptional uniformity are among the features that make amorphous magnetic materials attractive for technology. Here it is shown that the magnetization reversal in amorphous SmCo thin films takes place through the formation of giant magnetic domains, over a centimeter across. The domain structure is found to be dictated by the direction of the imprinted in-plane easy axis and the film boundaries. This is a consequence of the size of the anisotropy and the structural uniformity of the films, which also allows the movement of millimeter-long domain walls over distances of several millimeters. The results demonstrate the possibility of tailoring the magnetic domain structure in amorphous magnets over a wide range of length scales, up to centimeters. Moreover, they highlight an important consequence of the structural perfection of amorphous films.

DOI: [10.1103/PhysRevB.89.224420](https://doi.org/10.1103/PhysRevB.89.224420)

PACS number(s): 61.43.Dq, 75.50.Kj, 75.70.Kw, 85.70.Kh

I. INTRODUCTION

Control of magnetic domain structure is important for a variety of applications such as magnetic memories [1] and magnetic logic circuits [2]. In any such scheme it is crucial to maximize the domain-wall mobility in order to allow fast and energy efficient manipulation of wall locations [3,4]. This involves minimizing extrinsic pinning by structural defects such as dislocations, grain boundaries or surface roughness. In addition, the domain structure should be determined entirely by design parameters such as the geometry of the device and not by the above-mentioned imperfections. The ability to tune the size and direction of the magnetic anisotropy of the material would also introduce another dimension to the design of domain-wall-based devices.

Amorphous magnetic films are highly interesting in this respect. Amorphous layers are uniform and smooth due to the absence of atomic steps, defects, and grain boundaries, which results in small domain-wall pinning [5]. Their magnetic properties are highly tunable [6] as compositions can be varied over a large range without having to consider changes in lattice constants. This facilitates layering with materials of widely different compositions in magnetic heterostructures [7–9]. In addition, it is possible to imprint an in-plane uniaxial anisotropy in amorphous layers, in an arbitrary direction, by applying a magnetic field during growth [10,11]. Hence, it is clear that amorphous magnetic films have immense potential for use in magnetic domain technologies.

Typical magnetic domain sizes in thin films are in the micrometer regime, although large quasi-single-domain states have been achieved by exchange coupling soft magnetic layers to a synthetic antiferromagnet heterostructure [12,13]. Here we uncover macroscopic magnetic domains in single amorphous SmCo thin films, without the use of a pinning layer. To capture the macroscopic nature of the domains we perform large-area Kerr imaging of the entire film area ($10 \times 10 \text{ mm}^2$), which reveals domains over a centimeter across, defined entirely

by intrinsic film properties, with domain walls moving over distances of several millimeters.

II. EXPERIMENT

The samples were grown by dc magnetron sputtering in a chamber with a base pressure below 7×10^{-10} mbar. The sputtering gas was Ar of 99.9999% purity and the growth pressure was 2.7×10^{-3} mbar. Si(100) substrates with the native oxide layer ($\sim 2 \text{ nm}$) were used, 0.5 mm thick and with an area of $10 \times 10 \text{ mm}^2$. The substrates were annealed in vacuum at $550 \text{ }^\circ\text{C}$ for 30 min prior to growth in order to remove surface impurities. First, a 2-nm-thick buffer layer of AlZr was deposited on the substrate from an $\text{Al}_{0.7}\text{Zr}_{0.3}$ compound target of purity 99.9%. The buffer layer promotes the formation of the amorphous phase of SmCo and facilitates wetting [8]. Then a 60-nm-thick SmCo alloy film was grown by cosputtering from 2-in. elemental targets of Co (99.9% purity) and Sm (99.9% purity). Finally, a 3-nm-thick capping layer of AlZr was grown to protect the SmCo layer from oxidation. All films were grown at room temperature, without any substrate cooling. A magnetic field of $\mu_0 H_{\text{im}} = 0.1 \text{ T}$ was applied during growth, using a sample holder equipped with two permanent magnets [10,14].

III. RESULTS AND DISCUSSION

The domain structure of SmCo films with compositions in the range 4–16 at.% Sm was studied, all showing qualitatively similar results and therefore we focus on the 4 at.% Sm sample in the following. To study the global magnetization reversal we have determined the magnetic domain structure of the entire sample surface using wide-field Kerr imaging [15], using both the longitudinal and the transverse Kerr effect. A subset of magnetic contrast images of the whole film area is shown in Figs. 1(a)–1(f), with the field swept parallel to the hard magnetic axis (the entire sequence of images can be found in Ref. [16], for samples containing 4 and 16 at.% of Sm). Giant magnetic domains are observed, more than a centimeter across, in a highly unusual pattern.

*fridrik.magnus@physics.uu.se

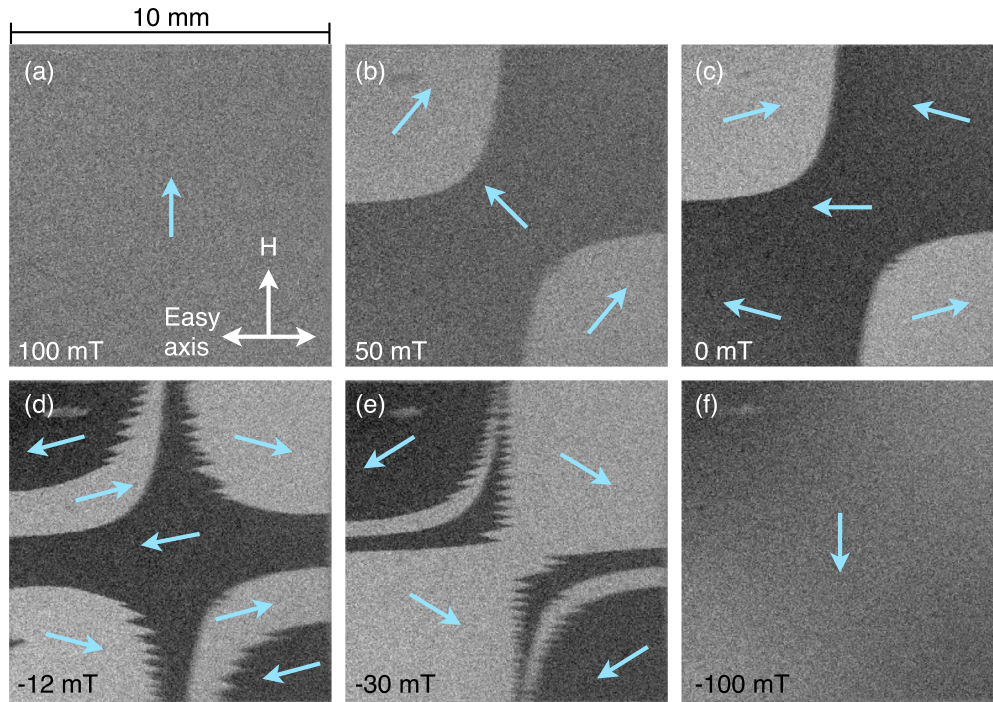


FIG. 1. (Color online) (a)–(f) Kerr images of the magnetic domain structure of a whole $10 \times 10 \text{ mm}^2$ $\text{Sm}_4\text{Co}_{96}$ film surface, recorded when sweeping the applied field parallel to the hard axis, from saturation in the up direction to saturation in the down direction. The blue arrows indicate the approximate magnetization direction of each domain. The images are taken in the transverse mode. Domains with diameters of over a centimeter are observed.

The films have a large, uniaxial in-plane anisotropy, which is imprinted during growth by applying a magnetic field [14]. For the film shown in Fig. 1, the in-plane anisotropy constant is $K = (3.9 \pm 0.4) \times 10^4 \text{ J/m}^3$. The nucleation of corner domains arises from a slight tilting of this imprinted easy axis in the corner regions of the film. This becomes apparent when the sample is demagnetized by applying an ac field with a decaying amplitude along the hard axis, as shown in Fig. 2(a). In this case, the magnetization breaks up into smaller domains, separated by 180° domain walls, which run parallel to the local easy axis. The tilting of the easy axis [see Fig. 2(b)] is a result of a small divergence of the imprinting field, as illustrated in Fig. 2(c), as well as the position-dependent demagnetizing fields that arise within the ferromagnetic film.

The hard-axis magnetization process is therefore as follows. When the field is reduced from saturation (100 mT), the magnetization starts to rotate towards the local easy axis. Due to the slight difference in the direction of the easy axis in the corners, quarter-circular domains are nucleated in two opposite corners where the magnetization has rotated in the opposite direction to that of the rest of the sample (50 mT). In zero applied field, the magnetization lies along the local easy axis over the entire sample, but in the two corners the magnetization is almost antiparallel to the rest of the sample. In a small positive field, the quarter-circular domains are switched by the nucleation and growth of domains with the opposite easy-axis magnetization direction, as this direction has a small component in the direction of the applied field (-12 mT). At a similar field, domains with a flipped magnetization are formed in the other two corners for the same reason. This flipping of the magnetization and the associated domain-wall motion is a

result of the strong preference of the magnetization to lie along the local easy axis due to the high anisotropy. With increasing positive field the magnetization rotates towards the applied field until saturation is reached (-100 mT). The pair of corners where the domains nucleate is determined by the direction in which the bulk of the sample magnetization starts to rotate and can therefore be selected by the direction of misalignment of

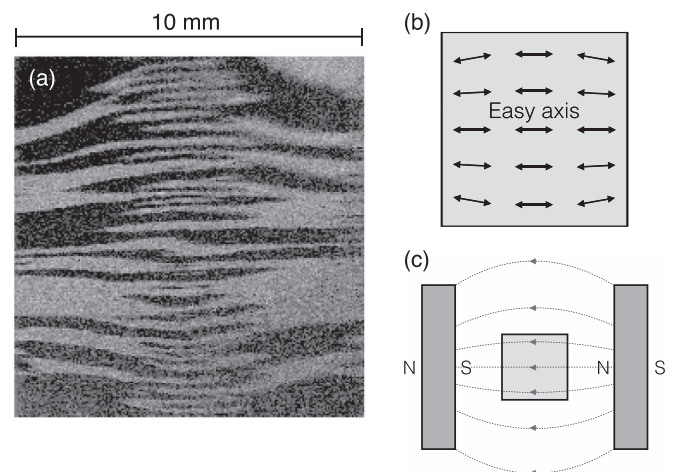


FIG. 2. (a) Kerr image of a $10 \times 10 \text{ mm}^2$ SmCo film after ac demagnetizing in the hard direction, showing a tilting of the anisotropy axis in the corner regions. (b) Schematic of the induced anisotropy axes. (c) Schematic illustration of the external growth field produced by two bar magnets (disregarding demagnetizing effects), demonstrating the small field inhomogeneity.

the applied field with respect to the hard axis. The domain sizes and shapes are quite sensitive to small changes in the applied field direction. The largest corner domains are obtained with the field exactly parallel to the hard axis.

Another feature observed in the images is the formation of zigzag domain walls. The zigzag shape is characteristic of charged domain walls that can appear in thin films with a large magnetic anisotropy where the shape serves the purpose of reducing the magnetic charge density [15,17,18]. A very coarse zigzag shape is observed in the corner domains nucleated at small negative fields, as seen in Figs. 1(d) and 1(e), and the zigzag shape appears to be only in the regions of the domain walls where the magnetization is head-on. The walls present at zero field [Fig. 1(c)] are also head-on and should therefore also be zigzag folded, although they appear to be straight in Fig. 1. Figure 3 shows a sequence of high-resolution images of these domain walls (which appear smooth in Fig. 1), which shows that they are indeed also zigzag folded but have a much finer structure. This is because these domain walls are created by rotational processes that are closer to equilibrium, in contrast with the coarse zigzag domain walls in Fig. 1, which are created by nucleation and wall motion. With increasing field (in the positive direction) the zigzag domain walls become coarser as the magnetization rotates towards a head-on configuration.

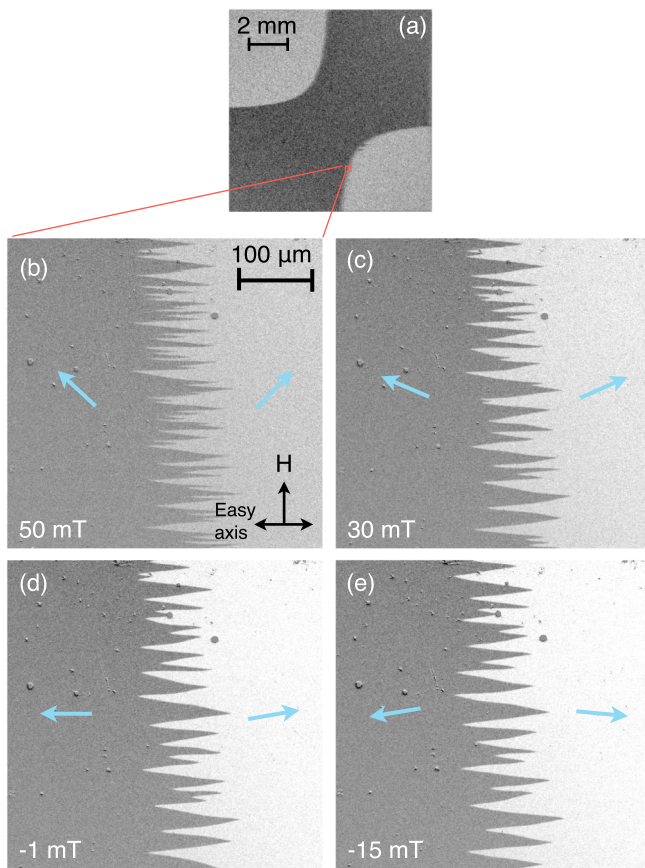


FIG. 3. (Color online) Kerr microscope images, taken in the transverse mode, showing the coarsening of zigzag domain walls. The arrows show the approximate direction of magnetization within the two domains. (a) Overview image showing the approximate location of (b)–(e) the high-resolution images.

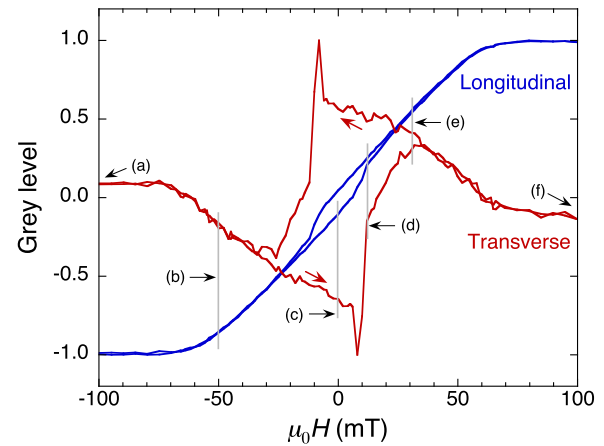


FIG. 4. (Color online) Hard-axis magnetization loops obtained from Kerr microscope images by integrating over the entire sample area, for both the transverse and longitudinal configurations. The curves are normalized to the maximum intensity. The points on the magnetization curves corresponding to the images in Fig. 1 are labeled (a)–(f). The domain-wall motion is barely visible in the longitudinal data, but very clear in the transverse data.

This is also clear from the increase in contrast between the two domains.

Figure 4 shows the magnetization loops obtained by integrating the sequence of images partially shown in Fig. 1. In the transverse configuration the signal is proportional to the component of magnetization perpendicular to the applied field and is therefore approximately zero at saturation. As the field is increased from -100 mT this perpendicular component of magnetization follows the lower path through zero applied field. The smooth variation of the magnetization in this region means that a magnetization rotation is taking place, without significant domain-wall motion. In a small opposite field the magnetization increases abruptly as the flipped corner domains emerge by the rapid movement of domain walls. Figure 4 also shows the loop obtained in the longitudinal configuration where the magnetization component parallel to the applied field is measured. This component of magnetization appears to rotate almost continuously during the field sweep except for a small opening at low field. The opening corresponds to the fields at which the domain-wall motion in the corner domains occurs and could be due to a small misalignment between the sensitivity axis and the applied field. This means that the domain structure is actually barely visible in the conventional longitudinal measurement geometry and from such a hysteresis measurement one could easily falsely conclude that the magnetization reversal takes place by a simple coherent rotation of the moments.

The domain structure observed here is in strong contrast with the intricate multidomain state typically observed in a hard-axis magnetization cycle on thin films with a uniaxial anisotropy. In polycrystalline films, the fine domain structure forms as a result of a statistical perturbation in the anisotropy of the crystal grains, known as *ripple* [15,19]. The high-resolution Kerr microscopy (as seen, for example, in Fig. 3) does not reveal any evidence of ripple in our films on the length scale of a few micrometers or above. Furthermore, the immense

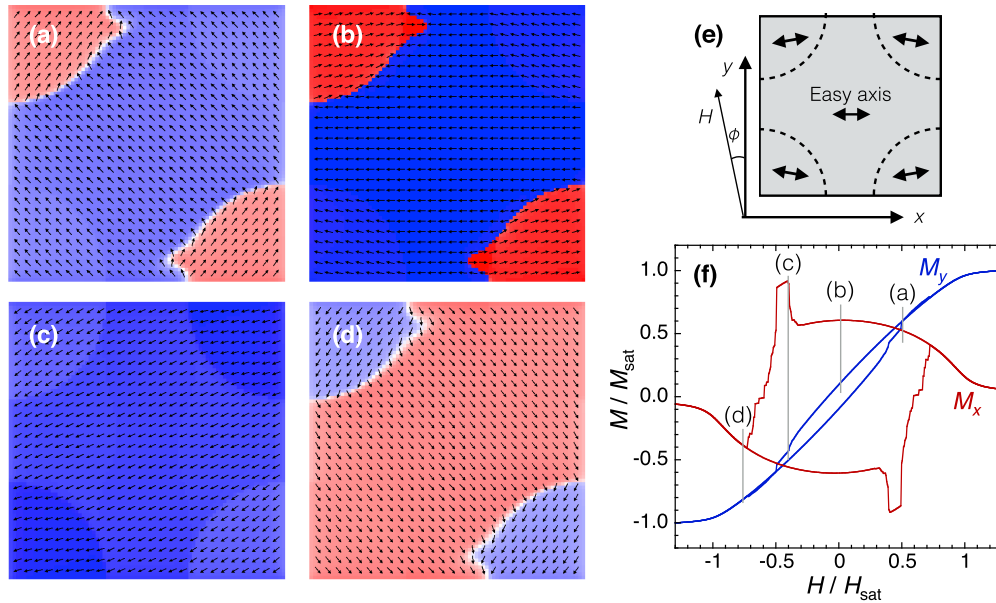


FIG. 5. (Color online) (a)–(d) Micromagnetic simulations revealing the role of the tilting of the anisotropy in domain formation. Calculations were performed on $800 \times 800 \text{ nm}^2$ square elements. A uniaxial anisotropy, pointing as shown in (e), was assumed and the field H was applied at an angle of $\phi = 1^\circ$ to the y axis. (f) Longitudinal M_y and transverse M_x components of the simulated magnetization with labels showing which positions on the magnetization curve correspond to the domain patterns in (a)–(d).

size of the observed domains indicates the absence of ripple and is a testament to the chemical and structural uniformity of the films in combination with the large imprinted anisotropy. This uniformity is characteristic of the amorphous structure and the layer-by-layer-like growth mechanism that produces films with very low roughness and small thickness variations, as demonstrated by x-ray scattering and transmission electron microscopy [14]. The amorphous AlZr buffer layer is crucial both for promoting the amorphous structure and wetting of the substrate [8,9]. Indeed, other studies of amorphous SmCo films grown without such a buffer layer have not shown large-area domains [18]. This is most likely due to the presence of nanocrystallites, which have a strong tendency to form at interfaces with oxides and ceramics and are difficult to detect with standard x-ray-diffraction techniques. Such nanocrystallites can have a marked effect on the magnetic properties of materials such as the magnetization and anisotropy [9], which are fundamental in determining the energy cost of domain formation. Furthermore, nanocrystallites can act as pinning sites for domain walls as well as result in an increased surface roughness [20], which can also increase the coercive field. It is therefore clear that small differences in nanostructure and morphology will strongly impact the magnetic domain structure.

The role of the tilting of the imprinted anisotropy axis was further investigated using micromagnetic simulations [21] shown in Figs. 5(a)–5(d). In order to describe the domain-wall energy correctly, a cell size of the order of a nanometer is needed (dictated by the spacial extent of the exchange interaction) as well as a total element size of centimeters, as this is the observed length of the domain walls. Furthermore, to model the true dipolar effects a $10 \times 10 \text{ nm}^2$ element is needed. As full-scale simulations of such $10 \times 10 \text{ nm}^2$ regions are not possible, the simulations were performed for $800 \times 800 \text{ nm}^2$

square elements with a thickness of 40 nm. There is no simple scaling criterion for the magnetization, exchange constant, and anisotropy and so the reduced element size implies that the energy of the model system is not fully representative of the measured films and absolute parameter values are not reliable. Therefore, the calculations were performed for several sets of parameters and the domain patterns compared on a qualitative basis. The divergence of the anisotropy, seen in Fig. 2, was mimicked by defining quarter-circular regions at the corners of the square wherein the angle of the uniaxial anisotropy axis was tilted by 14° , as shown in Fig. 5(e). A small offset was used between the applied field and the hard axis to lift the degeneracy in the domain formation.

Using an anisotropy constant of $K_u = 2 \times 10^6 \text{ J/m}^3$ and magnetization and exchange constant values consistent with Co ($M_s = 1400 \text{ kA/m}$ and $A = 20 \times 10^{-12} \text{ J/m}$, respectively), the reversal process obtained in the simulations is in good agreement with the Kerr imaging. As the field is reduced from saturation, two corner domains are formed, which remain largely unchanged through zero field. In a small reversed field range the sample is in a single-domain state before the corner domains reemerge with a reversed magnetization. The nucleation of reversed domains with the associated domain-wall motion [Figs. 1(d) and 1(e)] is not observed in the simulations, nor are the zigzag domain walls, but this is to be expected as the simulations cannot capture the huge range of relevant length scales. Nonetheless, both the longitudinal M_y and transverse M_x magnetization loops obtained by simulations, seen in Fig. 5(f), are strikingly similar to the measured hysteresis loops in Fig. 4. Here M_y shows a linear behavior, with a small opening around zero field, whereas M_x shows a large hysteresis with spikes where the flipping of the corner domains occurs. Therefore, despite the downscaling of the problem, the simulations seem to

capture most of the macroscopic features of the system. If the tilting of the anisotropy axis in the corner regions is removed and a uniform anisotropy axis assumed, we obtain a single-domain rotation of the magnetization, as the field is reduced from saturation to remanence. For smaller values of anisotropy, the element breaks up into smaller domains, in a flux closure-type arrangement, where the magnetization is parallel to the element edges. Therefore, we can conclude that the large anisotropy in combination with a tilted anisotropy axis in the corner regions is the driving force behind the experimentally observed domain patterns.

IV. CONCLUSION

We have demonstrated that macroscopic magnetic domains (centimeters across) are found in amorphous SmCo thin films with an imprinted anisotropy. Experimental identification of domains of this size requires large-area Kerr imaging and more local probes of magnetization, or even global measurements of the longitudinal magnetization component, may give an incorrect picture of the magnetic response. Furthermore, the large domain size presents a problem for micromagnetic simulations. Capturing the essence of the magnetic response requires a vast range of length scales, from nanometers to

centimeters. This is not possible with current techniques and calls for the development of new methods for dealing with such multi-length-scale problems.

We have found that the giant domains are a result of a large imprinted magnetic anisotropy and exceptional structural uniformity that result in the absence of domain ripple and extrinsic domain-wall pinning. Corner domains are formed due to a slight tilting of the local anisotropy axis, but simulations indicate that eliminating the tilting would result in a single-domain coherent rotation of magnetization. Consequently, it should be possible to design domain sizes and shapes at will over length scales ranging from nanometers to centimeters by patterning a single amorphous magnetic film, without the need for complex heterostructures. This is an intriguing prospect for magnetic domain technologies.

ACKNOWLEDGMENTS

The authors would like to thank Stefan Pofahl for his assistance in performing the Kerr imaging. This work was funded by the Swedish Research Council, the Knut and Alice Wallenberg Foundation, the Carl Trygger Foundation, and the Swedish Foundation for International Cooperation in Research and Higher Education.

-
- [1] S. S. P. Parkin, M. Hayashi, and L. Thomas, *Science* **320**, 190 (2008).
 - [2] D. A. Allwood, *Science* **309**, 1688 (2005).
 - [3] T. Koyama, D. Chiba, K. Ueda, K. Kondou, H. Tanigawa, S. Fukami, T. Suzuki, N. Ohshima, N. Ishiwata, Y. Nakatani, K. Kobayashi, and T. Ono, *Nat. Mater.* **10**, 194 (2011).
 - [4] E. De Ranieri, P. E. Roy, D. Fang, E. K. Vehstedt, A. C. Irvine, D. Heiss, A. Casiraghi, R. P. Campion, B. L. Gallagher, T. Jungwirth, and J. Wunderlich, *Nat. Mater.* **12**, 808 (2013).
 - [5] E. S. Machlin, in *Materials Science in Microelectronics II: The Effects of Structure on Properties in Thin Films* (Elsevier, Amsterdam, 2010), p. 59.
 - [6] D. D. Djayaprawira, K. Tsunekawa, M. Nagai, H. Maehara, S. Yamagata, N. Watanabe, S. Yuasa, Y. Suzuki, and K. Ando, *Appl. Phys. Lett.* **86**, 092502 (2005).
 - [7] H. G. Cho, Y. K. Kim, and S.-R. Lee, *J. Appl. Phys.* **91**, 8581 (2002).
 - [8] C.-M. Choi, J.-O. Song, and S.-R. Lee, *IEEE Trans. Magn.* **41**, 2667 (2005).
 - [9] P. T. Korelis, A. Liebig, M. Björck, B. Hjörvarsson, H. Lidbaum, K. Leifer, and A. R. Wildes, *Thin Solid Films* **519**, 404 (2010).
 - [10] H. Raanaei, H. Nguyen, G. Andersson, H. Lidbaum, P. Korelis, K. Leifer, and B. Hjörvarsson, *J. Appl. Phys.* **106**, 023918 (2009).
 - [11] G. Suran, M. Naili, and J. Sztern, *J. Appl. Phys.* **63**, 4318 (1988); G. Suran, M. Naili, H. Niedoba, F. Machizaud, O. Acher, and D. Pain, *J. Magn. Magn. Mater.* **192**, 443 (1999).
 - [12] K. Tanahashi, A. Kikukawa, N. Shimizu, and Y. Hosoe, *J. Appl. Phys.* **91**, 8049 (2002).
 - [13] H. S. Jung and W. D. Doyle, *IEEE Trans. Magn.* **38**, 2015 (2002).
 - [14] F. Magnus, R. Moubah, A. H. Roos, A. Kruk, V. Kapaklis, T. Hase, B. Hjörvarsson, and G. Andersson, *Appl. Phys. Lett.* **102**, 162402 (2013).
 - [15] A. Hubert and R. Schäfer, *Magnetic Domains: The Analysis of Magnetic Microstructures* (Springer, New York, 2000).
 - [16] See Supplemental Material at <http://link.aps.org/supplemental/10.1103/PhysRevB.89.224420> for a sequence of images.
 - [17] V. Madurga, J. Vergara, and C. Favieres, *J. Magn. Magn. Mater.* **272–276**, 1681 (2004).
 - [18] M. Gronau and S. Methfessel, *IEEE Trans. Magn.* **17**, 3105 (1981).
 - [19] B. D. Cullity and C. D. Graham, *Introduction to Magnetic Materials*, 2nd ed. (Wiley, Hoboken, 2008).
 - [20] A. Liebig, P. T. Korelis, H. Lidbaum, G. Andersson, K. Leifer, and B. Hjörvarsson, *Phys. Rev. B* **75**, 214202 (2007).
 - [21] M. J. Donahue and D. G. Porter, OOMMF User's Guide, Version 1.0, NISTIR Interagency Report No. 6376 (National Institute of Standards and Technology, Gaithersburg, 1999), <http://math.nist.gov/oommf>